



HAL
open science

Multiscale topology optimization of 3D structures: A micro-architected materials database assisted strategy

Tristan Djourachkovitch, Nawfal Blal, Nahiene Hamila, Anthony Gravouil

► To cite this version:

Tristan Djourachkovitch, Nawfal Blal, Nahiene Hamila, Anthony Gravouil. Multiscale topology optimization of 3D structures: A micro-architected materials database assisted strategy. *Computers & Structures*, 2021, 255, pp.106574. 10.1016/j.compstruc.2021.106574 . hal-03660006

HAL Id: hal-03660006

<https://hal.science/hal-03660006>

Submitted on 16 May 2023

HAL is a multi-disciplinary open access archive for the deposit and dissemination of scientific research documents, whether they are published or not. The documents may come from teaching and research institutions in France or abroad, or from public or private research centers.

L'archive ouverte pluridisciplinaire **HAL**, est destinée au dépôt et à la diffusion de documents scientifiques de niveau recherche, publiés ou non, émanant des établissements d'enseignement et de recherche français ou étrangers, des laboratoires publics ou privés.



Distributed under a Creative Commons Attribution - NonCommercial 4.0 International License

Multiscale topology optimization of 3D structures: A micro-architected materials database assisted strategy

Tristan Djourachkovitch ^a, Nawfal Blal ^{a,*}, Nahiene Hamila ^{a,b}, Anthony Gravouil ^a

This article presents a datadriven multiscale optimization method for solving 3D problems under given boundary conditions. The topology is represented by an extended level-set function that allows the nucleation of new holes throughout the process making it less sensitive to the initial guess. The two scales involved are the structural (macro) scale and the material (micro) scale. For the macro scale, the stiffness is maximized while reducing the weight of the structure; while for the micro scale, the homogenized elasticity tensor is prescribed and the weight is also minimized. In order to decrease the significant computational cost of multi-scale optimization, a datadriven approach is proposed. The method consists in two main steps: (1) an offline step to build a database (catalog of optimal micro-architected materials indexed by their effective elasticity) for a wide range of desired elasticity tensors, and (2) an online step aiming to optimize the 3D structure at the macroscale. The precomputed catalog is thus interrogated in order to find the best micro-architected material within the macroscale optimization. This method performs a two scales weight minimization and leads to a significantly light structure design. The optimization formulation is first introduced. Then a few 3D benchmark tests are given for the multi-scale optimization using micro-architected materials.

1. Introduction

Design optimization consists in optimizing some specified properties by modifying the shape or the topology of the admissible domain considered. Therefore the optimization problem is replaced by a material distribution problem. Design optimization has received significant attention in the past decade and is still a subject of great interest not only in research but also in the industry. For many engineering applications, especially those involving dynamics, reducing structures weight while preserving suitable mechanical properties is a key issue. Design optimization is well suited to improve the shape but often leads to complex topologies. The recent breakthroughs in additive manufacturing processes have proven the efficiency of those techniques through many successful industrial [1] and research [2–4] applications to design such complex shapes.

From the pioneering work of Kikuchi and Bendsøe [5] concerning structural optimization, the field of applications of design opti-

mization has significantly expanded covering extensive areas such as mechanics, thermo-mechanics [6,7], acoustic [8,9], etc. At the same time, the field of materials science has shown the potential of architected materials such as composite materials and foams to improve some properties at the lower scale as the stiffness or the weight of these materials. The ability to manufacture such materials with specific architecture or/and micro-architecture has led to considering different scales in design optimization [10]. The two separated scales that are mainly considered are the macro or effective scale which depends on the dimension of the domain (structure) that is optimized, and the microscale that is the scale of the material used within the macro-structure. Many studies have been conducted focusing on the macro [11–16] or the micro [17,6,18–20] scale. A variety of paper lately investigated the potential of concurrent macro/micro design optimization [21–26] where a periodic micro-architected material is optimized within the structure that is optimized as well. One can find different approaches making use of a unique micro-structure or a distribution of different materials within specific areas of the macro-structure [27,28]. Several methods in the literature to perform design optimization can be consulted in [29]. Density approaches, such as the SIMP (Solid Isotropic Material with Penalization) method [30], use a density function as the design variable. For sta-

* Corresponding author.

E-mail addresses: tristan.djourachkovitch@insa-lyon.fr (T. Djourachkovitch), nawfal.blal@insa-lyon.fr (N. Blal), hamila@enib.fr (N. Hamila), Anthony.Gravouil@insa-lyon.fr (A. Gravouil).

bility issues, the density function is piecewise continuous and is penalized to strengthen the so called “black and white” design. This formulation generally uses an optimality criterion [31] based on the derivative of the objective function with respect to the design variables. The evolution of the design throughout the optimization process is guided by the evolution of the density function that can evolve smoothly from the solid (density of one) to the void (density of zero) phase and vice versa. As new holes can appear and existing ones can collapse or merge with others, this method can perform topology changes and therefore is a topology optimization method.

Other methods such as topological derivative [18,12] based on the exact formulation of the derivative of the objective function with respect to the nucleation of circular inclusions or MMC (moving morphable components) [32] have proven themselves to be well suited to perform topology optimization.

Another approach consists in using a level-set function [33,34] to implicitly represent the interfaces between the void and the solid phases. This method is usually coupled with the shape derivative theory [35] that enables to find a gradient based direction to decrease the so called objective or cost function. The level-set function is then updated using the evolution of the gradient. A critical issue with this approach is that the evolution of the level-set is only defined on the interfaces between the solid and the void phase and can not create new interfaces. Even though already existing holes can merge together, new ones can not be created with the standard method making it very sensitive to the initial topology used for the optimization process [11]. Allaire et al. [12] proposed a coupling between shape derivative and topological derivative to provide topology changes in the shape optimization framework and therefore relax the set of admissible topology for the design optimization. Wang et al. [15] proposed an extended computation of the velocity field to perform topology changes within the shape optimization framework. Yamada et al. [14,36] proposed to incorporate a fictitious interface energy derived from the phase field concept in the level-set formulation.

This article presents a level-set based method to design both micro-architected materials with predefined constitutive behavior and the macroscale structure topology. It is a multi-scale optimization problem since the objective for the microscale is to find the adequate design of the local micro scale unit cell whose homogenized, or macro, behavior meets the prescribed desired behavior. Integrating the results of the topological optimization prescribing the effective stiffness tensor with advanced additive manufacturing processes is in complete adequacy with the Milton and Cherkaev remarks confirming that “...any given positive fourth order tensor satisfying the usual symmetries of elasticity can be realized as the effective elasticity tensor of a two-phase composite comprised of a sufficiently compliant isotropic phase and a sufficiently rigid phase configured in an suitable microstructure” [37,38]. Following the idea of Ferrer et al.[39], a broad range of micro-architected materials is computed in a first off-line step to build a database of optimal materials. The database is then used in the on-line step where the macro structure is optimized while the best micro-architected material (in terms of rigidity and weight) is chosen within the precomputed catalog. The different scales involved in the proposed approach are illustrated in Fig. 1. At each integration point of the macro-structure, a representative volume element (RVE) is allocated. It corresponds to a periodic micro-architected material whose homogeneous mechanical behavior is equal to the one of the smallest periodic pattern one can identify in the material. The representative cell element (RCE) scale is associated to this pattern. It is worth mentioning that the scale of the pattern (RCE) and the scale of the material (RVE) can be separated especially if the number of duplication of the pattern is significant. However, since the pattern is periodic, its homogeneous behavior

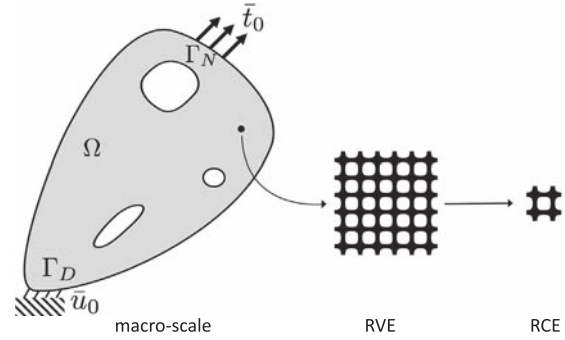


Fig. 1. The three different scales involved in the proposed optimized multiscale approach, namely the macro (left), the micro or RVE (middle) and the cell or RCE (right) scale. Since the RVE consists in a duplication of the RCE, the scales of the material and the cell are confounded thereafter.

is equal to the one of the material and from the homogenization point of view, there is technically no differences between those two scales. Therefore, the distinction is no longer made in the paper and the optimization of micro-architected material that is presented is made on a single pattern. Furthermore, to ensure scale separation assumption of the homogenization theory that will be used in the sequel, the same micro-architected material is selected for all the macro structure since the periodicity assumption is necessary to compute the homogenized behavior of the material.

The two-scales (macro/micro) optimization method leads to significant weight reduction. The benefit of the use of a catalog of optimized materials is that once a consistent database is computed, any multi-scale problem can be solved with minor computation cost related to the macro scale optimization. The combination of multiscale modeling and synergistic database driven strategies is a promising key ensuring optimal designs with acceptable time computations. The main contributions of the present works lie in:

1.1. Adopting a two scale topology optimization with compliance and weight minimization

The studied two-scales optimization problem is considered adopting the minimization of the structure compliance and its weight. The goal is the minimization of the objective function which is a weighted sum of the mechanical and weight performances. The weight minimization is directly integrated in the objective function and not considered as a constraint condition in the minimization problem (see for instance [11]). The idea of using multi-scale topology optimization is admittedly not new. Herein, the final topology and performance are obtained updating the design variables at different scales. The incorporation of the macroscopic topology (so the macroscale density) and the microscale material density as design variables is an original key that aims to significantly decrease the final weight of the structure. Use is made hereafter of unique microscale microstructure whereas the macroscopic topology can change over the optimization process. The scales separation assumption used for the mathematical development is so far respected without need to add the RVE scale into the consideration. The feature of optimizing with spatially varying microstructures still remains complicated. As stated in [40], enforcing the connectivity conditions can be achieved at expense of the desired performances.

1.2. Database driven two scales topology optimization

The originality of this work is to build a database of micro-architected materials using an original formulation that feeds

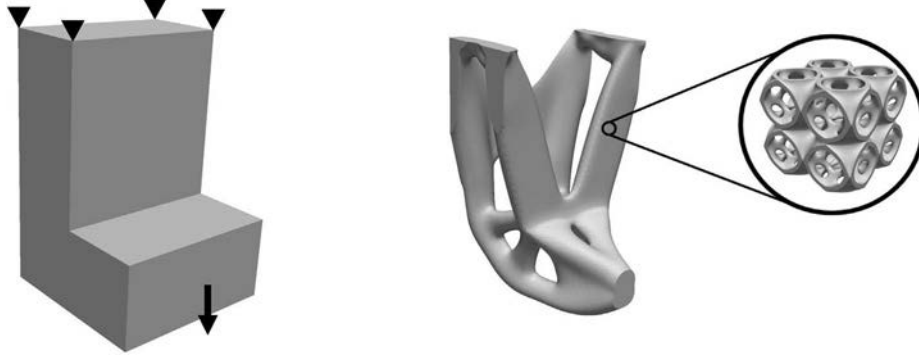


Fig. 2. The macroscopic optimization problem (left), its associated optimized macro structure (middle) incorporating the micro architected material (right).

the macroscale optimization to significantly decrease the computational time. The multiscale aspect is taken into account and time computations are accelerated thanks to an offline-online paradigm. At the offline stage, a catalog of different micro-architected materials with desired properties is built using a level-set local topological optimization. The catalog is used at the online stage for the topology optimization of the macroscopic structure problem. The database assisted strategy has the advantage to significantly reduce the two scales topology process. Moreover, the micro-architected materials catalog can be used independently of the considered macro-structure problem to be optimized. The idea of such approach is to reduce the multiscale topology optimization computations cost to only the macroscale computations cost. The microscale topology design of the micro-architected materials is done *once for all* at the offline stage and can be used after for any macro-structure problem. Some conceptual issues for the definition of the admissible microstructures to be built can be tackled too by the idea of data-driven approaches.

2. Multi-scale optimization framework

The objective of this work is to design high performance structures incorporating micro-architected materials. The multi-scale problem tackled here is illustrated in Fig. 2 where the left picture corresponds to the optimization problem with given boundary conditions, macroscopic loads and optimization domain. The right picture presents an optimal solution incorporating a micro-architected material.

The existing works on multiscale topology optimization structure can be classified into two families: optimization solvers aiming to minimize some physical quantities (compliance, displacement, ...) where the mass (or volume) is taken into account as a constraint [11,12], and topology optimization solvers based on the minimization of the structure mass (or volume) where the physical demands are imposed as constraints [41]. Our approach consists in meeting different design demands in the same cost function to be minimized. The user has to fix the weight to give to each design performance.

The multi-scale optimization problem consists in a compromise between minimizing the global compliance for single and deterministic load and the global solid phase ratio so the weight of the structure is significantly decreased while preserving suitable mechanical properties. It has been widely studied in the literature, one can find similar objective functions in [42,43] where the minimization functional is stated as:

$$\min_{\Omega} J = \int_{\Omega} \varepsilon(\mathbf{u}) : \mathbb{C}(\mathbf{x}) : \varepsilon(\mathbf{u}) d\Omega + \beta \int_{\Omega} d\Omega \quad (1)$$

$$\text{s.t. : } G(\mathbf{u}) = 0$$

where J is the objective function that is the sum of the global compliance (first term of Eq. (1)) and solid phase ratio of the structure (second term of Eq. (1)), G is an optimization constraint that stands for the mechanical equilibrium. The parameter $\beta [kg.m^{-1}.s^{-2}] \in \mathbb{R}^+$ is a scaling factor to enforce the homogeneity of (1) and sets the compromise between the two properties to optimize, D is the admissible domain and Ω stands for the topology of the structure, $\mathbb{C}(\mathbf{x})$ is the fourth order elasticity tensor of the constitutive law that describes the material behavior at the small scale and ε is the second order strain tensor.

Since the material heterogeneities introduced by the micro-architected material might be much smaller compared to the structure dimensions, a classical single scale optimization algorithm could be adequate because of the inherent finite element discretization. Indeed, to be able to capture micro-architected materials, one would have to use very thin meshes that might become prohibitive in terms of computation cost without using some specific advanced methods as in [44]. To overcome this significant issue, multi-scale techniques based on homogenization theory provide a suitable framework. The underlying idea is that the overall problem might be separated into two sub-problems, namely the macro and the micro scale problem that interact with each other using average operators for the small heterogeneities. To solve the micro scale problem, appropriate boundary conditions are required. One can find in the literature different sets of boundary conditions such as kinematic boundary conditions, static boundary conditions and periodic boundary conditions [45]. In the context of first order homogenization, the local fields fluctuate around their mean value due to the periodicity of the heterogeneities. The additive decomposition of the displacement field (also called scale separability assumption) is then expressed as [39,45,46]:

$$\mathbf{u} = \bar{\mathbf{u}} + \tilde{\mathbf{u}} \quad (2)$$

where the local displacement field solution \mathbf{u} is assumed to be split into a macroscopic counter part $\bar{\mathbf{u}}$ that depends on the macroscopic boundary conditions, and a microscopic counter part $\tilde{\mathbf{u}}$ that captures the behavior of the heterogeneities at the small scale. Since $\tilde{\mathbf{u}}$ is assumed fluctuating over the unit cell, periodic boundary conditions are applied: $\tilde{\mathbf{u}}(\mathbf{x}^+) = \tilde{\mathbf{u}}(\mathbf{x}^-), \forall (\mathbf{x}^+, \mathbf{x}^-) \in \partial\Omega^+ \times \partial\Omega^-$ where $\partial\Omega^+$, et $\partial\Omega^-$ are respectively the opposite sides of the cell Ω . The compatibility equation of this hierarchical decomposition leads to $\varepsilon = \nabla_s \bar{\mathbf{u}} + \nabla_s \tilde{\mathbf{u}}$. The periodicity of the fluctuation field $\tilde{\mathbf{u}}$ makes the average¹ of its associated strain over Ω straightforwardly vanish, i.e. $\langle \nabla_s \tilde{\mathbf{u}} \rangle_D = 0$, so that $\langle \varepsilon \rangle = \langle \nabla_s \bar{\mathbf{u}} \rangle = \bar{\varepsilon}$. With this assumption in hand, one can perform a two scales optimization where the macro

¹ the average operator over a RVE Ω reads $\langle \bullet \rangle_{\Omega} = \frac{1}{|\Omega|} \int_{\Omega} \bullet d\Omega$.

(resp. micro) scale is optimized referring to $\bar{\mathbf{u}}$ (resp. \mathbf{u}) [21,23,38]. An illustration of this two scales problem is given in Fig. 3 where it is indicated that, for elastic materials, the dialogue between the macro and the micro scale is driven by two ingredients:

1. from the macroscale to the microscale: the local macroscopic strain field $\bar{\boldsymbol{\varepsilon}}$
2. from the microscale to the macroscale: the homogenized elasticity tensor \mathbb{C}^H

Full topology optimization computations integrating two scales (blue box in Fig. 3) still implies a substantial computation effort since the overall number of design variables becomes the product of integration points at the macro scale and the discretization at the micro scale. For the complexity estimation, if the macro-structure is sampled into N^{mac} macro elements and each macro element contains a microscale material with N_N^{mic} elements, the total number of the multiscale topology optimization design variables is $N^{\text{mac}} \times N^{\text{mic}}$ using the standard full two-scale topology optimization solver. This becomes computationally unaffordable especially for 3D structures. To minimize the computational effort and be able to perform multi-scale topological optimization of structures incorporating micro-architected materials, the method proposed in this work consists in using a precomputed database of optimized micro-architected materials as proposed in [39] (red box in Fig. 3). The preliminary step so called 'off-line step' consists in optimizing a wide range of a micro-architected materials with different properties (that will be discussed in the sequel) and store them in the database. Hereafter the term 'catalog' refers to this precomputed database of micro-architected materials indexed by their homogenized stiffness tensor. It gives a direct mapping from the effective elastic properties and the associated micro-structure and the underlying solid phase ratio. Once the database is sufficiently enriched, the multi-scale optimization problem, can be performed using the catalog in the so-called 'on-line step'. The main advantage of this method is to significantly decrease the number of design variables during the on-line step, and thus, allow to use relatively thin meshes even for 3D problems. Indeed, the multi-

scale topology design computation is reduced to only the macro-scale topology optimization cost with N^{mac} design variables. The effort done offline for the catalog construction is rewarded at the online stage since the catalog can be used for any macro-structure topology optimization problem.

This multi-scale optimization problem can finally be stated as:

$$\min_{\Omega, \mathbb{C}^H, \phi} J = \int_{\Omega} \boldsymbol{\varepsilon}(\bar{\mathbf{u}}) : \mathbb{C}^H : \boldsymbol{\varepsilon}(\bar{\mathbf{u}}) d\Omega + \beta \phi \int_D d\Omega \quad (3)$$

$$\text{s.t. : } G(\bar{\mathbf{u}}) = 0$$

where \mathbb{C}^H is the homogenized elasticity tensor of the micro-architected material and ϕ its solid phase ratio. The compliance-to-weight trade-off is fixed by the user with the β parameter.

It should be noted that the previous multi-scale optimization process is performed in two stages: at the macroscopic scale, the macro-topology Ω is optimized whereas the design variables (ϕ, \mathbb{C}^H) are results of a microscopic topology optimization process.

The originality of this work is to build a database of micro-architected materials with the homogenized elasticity tensor and the solid phase ratio as design variables. Each snapshot (ie: each micro-architected material stored in the catalog) is associated to a different elasticity tensor and solid phase ratio.

3. Formulation of the multi-scale optimization problem

As explained in Section 2, the strategy adopted for the multi-scale optimization is to separate the global problem into two sub problems namely the micro scale problem (off-line step) and the macro scale problem (on-line step). Details about the formulation are given in the sequels.

3.1. The off-line step: Micro-structure optimization with desired elasticity

The micro scale topological optimization. Let D^m be an open set of $\mathbb{R}^N, N \in \{2, 3\}$ that defines the microscopic design domain and

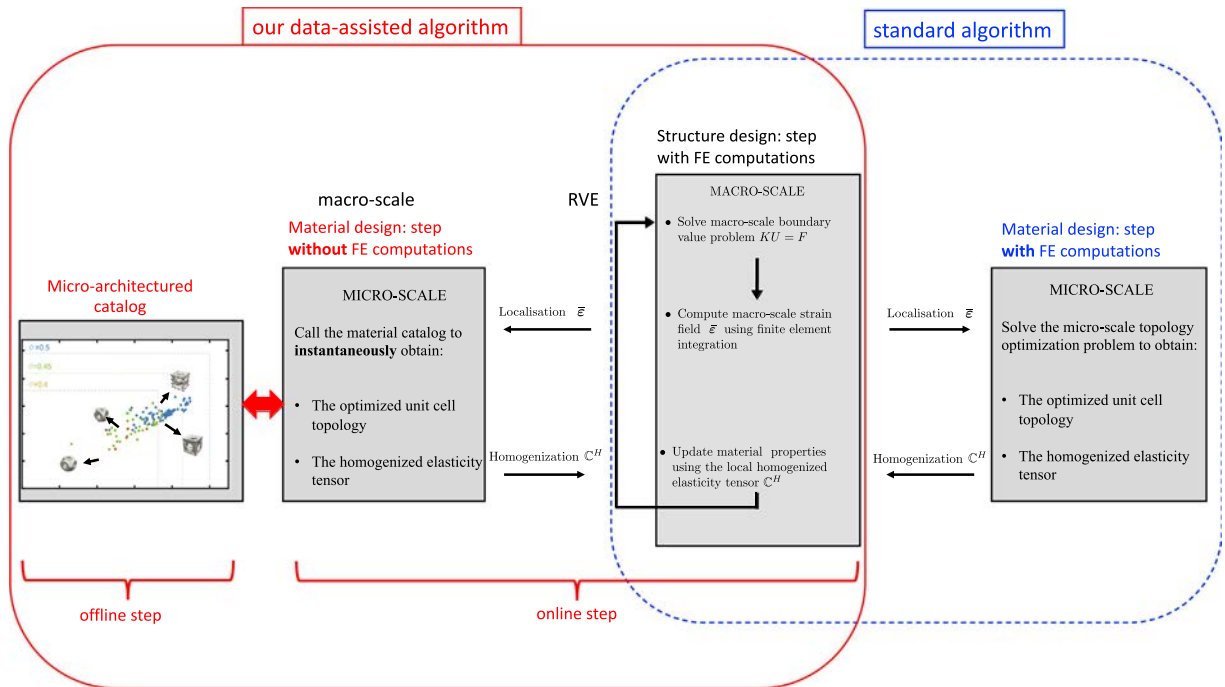


Fig. 3. Two-scales optimization problem.

Ω^m defines a subset of D^m denoting the solid phase. The topology optimization problem aims to *minimize the least square error between predefined and homogenized (or macroscopic) components of the elasticity tensor for an elastic body*. Similar problems have been studied in [17,6,47]. The optimization problem at the micro scale reads:

$$\min_{\Omega^m} J^m(\Omega^m) = \sum_{ijkl} \eta_{ijkl} \left(C_{ijkl}^H - C_{ijkl}^T \right)^2 \quad (4)$$

$$\text{s.t. : } \int_{\Omega^m} d\Omega^m < V_{max}^m$$

The right term of equation (4) is the least square error criterion where C_{ijkl}^H and C_{ijkl}^T stand respectively for the homogenized (or macroscopic) and target (or prescribed) components of the fourth order elasticity tensor and η_{ijkl} is a weight unit-less parameter (fixed by the user). The V_{max}^m parameter is a classical volumetric constraint on the unit cell that can be interpreted as a maximal admissible porosity at the micro scale. The optimization problem can be considered as an inverse homogenization problem and can be solved by a level-set topology optimization approach.

Denoting by \otimes the dyadic tensorial product and $(\mathbf{e}_i)_{i=1,2,3}$ the orthonormal vectors that shape the Euclidean physical space \mathbb{R}^3 , the homogenized components of the elasticity tensor \mathbb{C}^H in Eq. (4) can be expressed using the homogenization theory and the Hill-Mandel lemma as [48]:

$$\mathbb{C}^H = \left(\int_{\Omega^m} \varepsilon(\mathbf{u}^{(ij)}) : \mathbb{C} : \varepsilon(\mathbf{u}^{(kl)}) d\Omega^m \right) \mathbf{e}_i \otimes \mathbf{e}_j \otimes \mathbf{e}_k \otimes \mathbf{e}_l \quad (5)$$

where the notation $\mathbf{u}^{(kl)}$ ($k, l = \{1, 2, 3\}$) corresponds to the displacement field solution of the microscale periodic boundary value problem:

$$\begin{cases} \text{div}(\boldsymbol{\sigma}^{(kl)}) = \mathbf{0} & \text{on } \Omega^m \\ \mathbf{u}^{(kl)}(\mathbf{x}^+) - \mathbf{u}^{(kl)}(\mathbf{x}^-) = \bar{\boldsymbol{\varepsilon}}^{(kl)} \cdot (\mathbf{x}^+ - \mathbf{x}^-), & \forall (\mathbf{x}^+, \mathbf{x}^-) \in \partial\Omega_+^m \times \partial\Omega_-^m \\ \boldsymbol{\sigma}^{(kl)} = \mathbb{C} : \boldsymbol{\varepsilon}^{(kl)} \\ \bar{\boldsymbol{\varepsilon}}^{(kl)} = \frac{1}{2}(\mathbf{e}_k \otimes \mathbf{e}_l + \mathbf{e}_l \otimes \mathbf{e}_k), & \langle \boldsymbol{\varepsilon}^{(kl)} \rangle = \bar{\boldsymbol{\varepsilon}}^{(kl)} \end{cases} \quad (6)$$

with the fixed external applied load consisting in the macroscopic unit strain $\bar{\boldsymbol{\varepsilon}}^{(kl)}$. One has to solve six unit elementary periodic BVP (6) to have all the components of the effective stiffness tensor \mathbb{C}^H .

3.2. The on-line step: structure optimization with compliance and mass minimization

The multi-scale topological optimization. Let D^M be an open set of \mathbb{R}^N , $N \in \{2, 3\}$ that defines the macroscopic design domain and Ω^M defines a subset of D^M denoting the solid phase. The objective is to *minimize the compliance (i.e. maximize the stiffness) and minimize the weight (i.e. minimize the solid phase ratio)*. The optimization problem at the macro scale is defined in Eq. (3).

The elasticity tensor \mathbb{C}^H as well as the solid phase ratio ϕ in Eq. (3) of the microarchitected materials incorporated in the structure are directly extracted from the catalog. At each iteration of the multi-scale optimization, the macroscale topology evolves and the objective function is tested for each snapshot to select the optimal one following a given criterion. Therefore the optimal micro-architected material might change at each iteration. If so, the homogenized elasticity tensor and the solid phase ratio of the microscale is updated at the macroscale using the database.

3.3. Level-set

The topology is represented using a level-set function ψ that is positive inside the solid phase, negative in the void phase and of nil value on the interfaces:

$$\begin{cases} \psi(\mathbf{x}, t) > 0 & \forall \mathbf{x} \in \Omega \setminus \partial\Omega \\ \psi(\mathbf{x}, t) < 0 & \forall \mathbf{x} \in D \setminus \Omega \\ \psi(\mathbf{x}, t) = 0 & \forall \mathbf{x} \in \partial\Omega \end{cases} \quad (7)$$

The level-set function ψ is governed by the Hamilton-Jacobi equation:

$$\frac{\partial\psi}{\partial t}(\mathbf{x}, t) + V(\mathbf{x}, t) \|\nabla\psi(\mathbf{x}, t)\| = 0 \quad (8)$$

The admissible domain D is meshed once for all and the evolution of the level-set throughout the optimization process drives the topology advancement. The elements that are cut by the level-set are considered as Ersatz material with the following stiffness:

$$\mathbb{C}^{\text{Ersatz}} = \phi \mathbb{C}^{\text{solid}} \quad (9)$$

recalling that ϕ stands for the solid phase volumetric ratio.

It is worth mentioning that design optimization using level-set method usually only leads to shape optimization and not topology optimization because the velocity function V in the Hamilton-Jacobi Eq. (8) computed with the shape derivative theory is usually defined on the interfaces and not in the whole domain. To overcome this significant issue and add more flexibility in the design, a criterion based on the local objective function gradient is also added to allow the nucleation of new holes in areas where it is suitable [15].

3.4. Shape derivative

To perform the minimization of the cost functions $J^M(\Omega^M)$ and $J^m(\Omega^m)$ the shape derivative theory is applied. The standard method (see Appendix A for more details) can not be directly applied for the cost functions $J^M(\Omega^M)$ and $J^m(\Omega^m)$ because they depend on the macroscale displacement field \mathbf{u} (resp. micro scale displacement field \mathbf{u}) and those fields depend on the topology Ω^M (resp. Ω^m). To overcome this difficulty the method of C ea is applied [49]. It consists in replacing the objective function J by an augmented Lagrangian functional L accounting for the optimization problem constraints. Details about the shape derivative of the objective functions defined in Eqs. (4) and (3) are given respectively in Appendix B and C.

4. Micro-architected database assisted strategy

As mentioned in Section 2, the multiscale optimization problem considering scale separability illustrated in Fig. 2 still requires a high computational effort because the microscale design has to be optimized at each iteration of the macroscale optimization. To significantly decrease these prohibitive costs, a database method is proposed here. The idea is to optimize "a priori" a large number of different micro-architected materials for a wide range of behaviors, namely a wide range of combinations of homogenized components of the elasticity tensor defined in Eq. (4). As the objective function at the microscale defined in Eq. (4) stands for the homogenized components of the elasticity tensor, it is practical to use it as entry parameters for the catalog. Moreover, any multi-scale objective function involving multiscale equilibrium will require the homogenized elasticity tensor of the micro-architected material so that such a catalog would be suitable

for other objective functions at the macroscale than the compliance that is used herein.

The objective function defined in Eq. (4) allows to design any kind of materials only restricting the prescribed elasticity tensor to be symmetric and definite positive. For the most general case of fully anisotropic materials, the elasticity tensor has 6 independent parameters for two dimensional cases and 21 independent parameters for three dimensional cases. To build a consistent catalog one should consider a 6 (resp. 21) dimensional space to map for 2D (resp. 3D) cases, which would require a very large number of snapshots, especially for 3D cases. This remains a cumbersome task and is, to the authors knowledge, not exploited until now.

In order to lower the dimension of the material parametric space to map with microstructures, some specific symmetries have to be considered. For example, isotropic materials only have two independent parameters and thus, a mapping of microstructures for isotropic materials requires much less snapshots. However, as stated in [50], the higher the number of parameters the better the accuracy of the database but the number of snapshots becomes prohibitive. For 2D cases, authors in [50] point out that anisotropic catalogs give better results (for the compliance as objective function) than cubic catalogs, which themselves give better results than isotropic catalogs. Since we focus on 3D problems in this paper, the compromise is chosen to cubic materials with three independent parameters, namely the Young modulus (E^H), the Poisson ratio (ν^H), and the shear modulus (G^H).

Therefore all the materials designed in this work have prescribed homogenized elasticity tensors \mathbb{C}^H of cubic symmetry. Using the fourth order tensor spectral decomposition, the tensor \mathbb{C}^H can be given in the form [51,52]:

$$\mathbb{C}^H = 3k^H \mathbb{J} + 2\mu_a^H \mathbb{K}_a + 2\mu_b^H \mathbb{K}_b \quad (10)$$

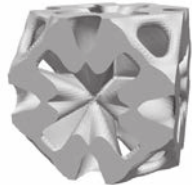
where (k^H, μ_a^H, μ_b^H) are the three independent material parameters standing respectively for the bulk modulus, the shear modulus over axes and the shear modulus in the axes. The tensors \mathbb{J} , \mathbb{K}_a and \mathbb{K}_b are elements of the basis of symmetric fourth order tensors with cubic symmetry. They are given by:

$$\begin{aligned} \mathbb{J} &= \frac{1}{3} \mathbf{i} \otimes \mathbf{i} \\ \mathbb{L} &= \mathbf{e}_1 \otimes \mathbf{e}_1 \otimes \mathbf{e}_1 \otimes \mathbf{e}_1 + \mathbf{e}_2 \otimes \mathbf{e}_2 \otimes \mathbf{e}_2 \otimes \mathbf{e}_2 + \mathbf{e}_3 \otimes \mathbf{e}_3 \otimes \mathbf{e}_3 \otimes \mathbf{e}_3 \\ \mathbb{K}_a &= \mathbb{L} - \mathbb{J} \\ \mathbb{K}_b &= \mathbb{I} - \mathbb{L} \end{aligned} \quad (11)$$

where \mathbf{i} is the second order identity tensor and \mathbb{I} is the symmetric fourth order unit tensor ($2I_{ijkl} = \delta_{ik}\delta_{jl} + \delta_{il}\delta_{jk}$). To be consistent with the material parameters (E^H, ν^H, G^H) used in the database, the following equations are recalled [53]:

$$E^H = \frac{9k^H \mu_a^H}{3k^H + \mu_a^H}, \quad \nu^H = \frac{3k^H - 2\mu_a^H}{6k^H + 2\mu_a^H}, \quad G^H = \mu_b^H \quad (12)$$

Table 1
Example of a snapshot stored in the database.

Material parameters	Optimized topology
$E = 0.240$ $\nu = 0.232$ $G = 0.076$ $V^m = 0.41$	

4.1. Multiparametric material database construction

The database contains $N^{\text{snap}} = 1000$ three dimensional snapshots and the maximal porosity ϕ is 0.5. The bulk base material used is assumed to be isotropic $\mathbb{C} = 3k\mathbb{J} + 2\mu\mathbb{I}$ and has arbitrary unitary Young modulus $E = 1$ Pa and Poisson ratio $\nu = 0.3$ (equivalently $k = 0.833$ Pa and $\mu = 0.385$ Pa). An example of a snapshot stored in the catalog is illustrated in Table 1. Each snapshot is indexed by four entry parameters: $k^H, \mu_a^H, \mu_b^H, \phi$ (equivalent to E^H, ν^H, G^H, ϕ).

The main difference of the present approach compared to the coupled macro/micro optimization method is to replace the expensive local topology optimization by a database assisted strategy. The set of corresponding design variables verifies the admissibility condition $(\phi, \mathbb{C}^H) \in \mathcal{U}_{\text{ad}}^{\mathbb{C}}$ where

$$\mathcal{U}_{\text{ad}}^{\mathbb{C}} = \{(\phi, \mathbb{C}) | \phi \in [0, 1] \text{ and } \mathbb{C} = \mathcal{H}(\mathbb{C}, \phi)\} \quad (13)$$

where \mathcal{H} is the homogenization operator that gives the effective elastic tensor for the micro-architected material obtained with the bulk elastic material \mathbb{C} having the density ϕ .

To explore the domain of admissible materials behavior, a detailed description of the design admissibility set $\mathcal{U}_{\text{ad}}^{\mathbb{C}}$ is of high importance. Indeed, for a given bulk medium with a volume fraction ϕ , the effective elastic tensors could be obtained with different corresponding micro-structures (no one-to-one relationship). This set of all possible homogenized elastic tensors at volume fraction ϕ , so-called *G-closure* set, has no detailed characterization: the existence or not of a micro-structure whose homogenized behavior corresponds to the fixed effective tensor is not guaranteed. The problem can be thus relaxed making use of the micromechanical Hashin-Shtrikman (HS) optimal bounds [54] obtained by a variational principle *a posteriori* database construction. Hence the definition of the set $\mathcal{U}_{\text{ad}}^{\mathbb{C}}$ can be reduced to the set of all possible (i.e. achievable) effective elastic tensors at volume fraction ϕ that respect the Hashin-Shtrikman bounds. The original HS bounds have been developed for effective isotropic stiffness media [54]. For the case of an effective stiffness tensor with cubic symmetry, use is made hereafter of the HS bounds obtained for a cubic effective behaviors resulting on a local isotropic bulk phase with microstructure cubic arrangements. These bounds are given in terms of the effective bulk modulus k^H and the effective equivalent shear modulus $(2\mu_a^H + 3\mu_b^H)/5$, namely [55,56]:

$$0 \leq k^H \leq k - \frac{1 - \phi}{\frac{1}{k} - \frac{\phi}{k + \mu}} \leq \frac{2\mu_a^H + 3\mu_b^H}{5} \leq \mu - \frac{1 - \phi}{\frac{1}{\mu} - \frac{\phi}{\frac{k+2\mu}{2\mu(k+\mu)}}} \quad (14)$$

A batch of $N^{\text{snap}} = 1000$ values of the triplet (k^H, μ_a^H, μ_b^H) respecting the cubic HS bounds has been selected randomly. The optimized topology corresponding to each point is then stored in the micro-architected materials catalog as a snapshot. It is worth mentioning

that for certain value of the triplet close to the theoretical bounds, the optimization process fails to reach the prescribed value since the characterization of \mathcal{W}_{ad}^C with HS bounds is not an exact characterization of the admissible behaviors that can be attainable by topological optimization. One can remark in Fig. 4 that the obtained snapshots do not cover all the domain bounded by the Hashin-Shtrikman bounds. The results obtained for the micro-architected materials topology optimization are illustrated in Fig. 4 for different volume fractions. All the obtained snapshots respect well the HS bounds but do not cover all the admissible domain in the parametric space $k^H - (2\mu_a^H + 3\mu_b^H)/5$. More particularly, zones with extreme properties or near the upper bounds are not attainable. Different reasons can explain this ascertainment. It is well known that the HS bounds are less accurate for the case of high contrasts between the mechanical properties of the solid phase and the void phase as pointed out in [54]. It is stated in [57] that the limits of the admissible domain can be more complex in the case of composites materials with a void phase. More important, it is well known that, contrary to the thermal properties, the Hashin Shtrikman bounds for elasticity problems do not characterize the set of all possible attainable effective tensors: there exist tensors satisfying these bounds which do not correspond to the effective behavior of a two phase material with proportional densities ϕ and $1 - \phi$ respectively. This mathematical point is still an open issue for mechanical problems.

However, even if the whole theoretical admissible domain is not explored and even if the final homogenized triplet lightly differs from the prescribed one, it still provides a snapshot in the admissible space so this approach using Hashin-Shtrikman bounds seems well-suited.

The issue of the precise definition of the set of possible effective tensors (see (13)) for the design variables of the multi-scale problem (3) is relaxed by the database assisted strategy thanks to the offline constructed catalog. Indeed, the optimization problem can be modified to the following form:

$$\begin{aligned} \min_{\Omega \subset D, (C^H, \phi) \in \mathcal{C}} J &= \int_{\Omega} \varepsilon(\bar{\mathbf{u}}) : C^H : \varepsilon(\bar{\mathbf{u}}) d\Omega + \beta \phi \int_{\Omega} d\Omega \\ \text{s.t. : } G(\bar{\mathbf{u}}) &= 0 \end{aligned} \quad (15)$$

where \mathcal{C} denotes the set of the all attainable effective elastic tensors corresponding to a micro-architected materials with density ϕ and that have been stored in the computational catalog. A representation of the database is given in Fig. (5). The precomputed snapshots are optimized setting the microscale problem (4).

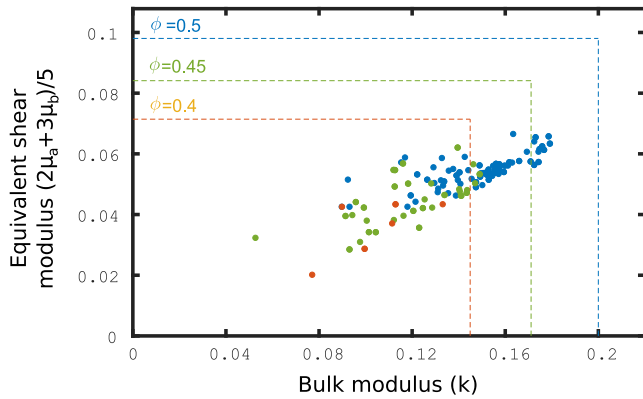


Fig. 4. Illustration of database within the Hashin-Shtrikman bounds for different values of ϕ . The color of the dots represents the volumetric ratio range. Blue: $\phi \simeq 0.5$, green: $\phi \simeq 0.45$ and yellow: $\phi \simeq 0.4$. (For interpretation of the references to color in this figure legend, the reader is referred to the web version of this article.)

It is clear that for the proposed method, the number of snapshots in the database will have an impact on the smoothness of the optimization process as well as on the final result. For the multiscale examples presented in the sequel, the admissible domain is sufficiently explored for the algorithm to reach the stopping criteria but enriching the database could lead to better results. A compromise has to be made between the computational cost of the exploration of the admissible domain and the accuracy of the multiscale optimization. The generation of more snapshots in the database is a significant way of improvement for future work.

4.2. Non-uniqueness and discretization

Topology optimization usually suffers from a certain number of numerical instabilities as stated in [58]. Among them one can notably mention mesh-dependency and non-uniqueness of the solution. To design the micro-architected materials several mesh sizes have been tested and the relative error between the homogenized and prescribed elasticity tensor is computed as follows:

$$e = \frac{\|C^H - C^P\|}{\|C^P\|} \quad (16)$$

where $\|\cdot\|$ is the Frobenius norm defined as $\|\mathbb{A}\|^2 = \mathbb{A} :: \mathbb{A}$ for a fourth order tensor \mathbb{A} .

Fig. 6 illustrates that, for the same prescribed elasticity tensor, the topology lightly depends on the mesh size and the relative error seems to decrease when increasing the number of elements. It seems reasonable to use at least 40^3 elements to optimize the

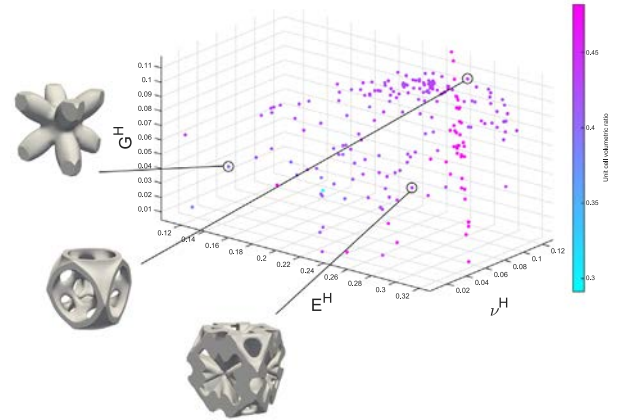


Fig. 5. Illustration of the catalog in the material space (E^H, ν^H, G^H) with some corresponding micro-architected materials.

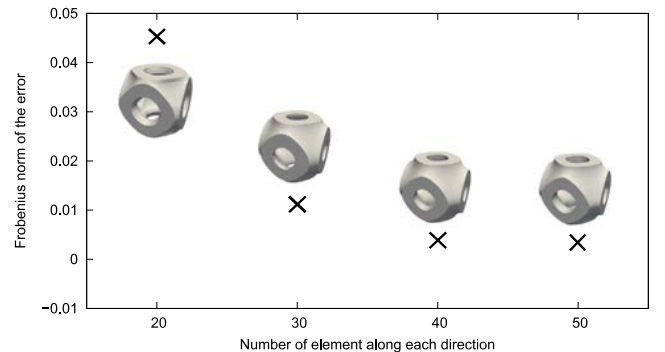


Fig. 6. Influence of the mesh size on the topology and the relative error for the same prescribed elasticity tensor.

microstructures. However, the special convergence is a current issue and the following papers [59,60] present some re-meshing techniques to achieve the spatial mechanical convergence while the topology changes. In this study the mesh is considered fixed *a priori* so the resulting minima are only meaningful on those grids.

As usually stated in gradient based minimization procedures, the evolution of the solution might get locked in some local minima and thus, the same optimization procedure starting from different initial guesses for the topology might lead to different results. This is even more observable for the non convex problem tackled in Eq. (4) since one can find different microstructures with the same elasticity tensor as illustrated Fig. 7.

4.3. Database driven macroscopic design

The concurrent data-driven macro/micro optimization algorithm using the precomputed database is illustrated in Algorithm 1. It is based on alternate directions method. The mechanical and design variables ($\bar{\mathbf{u}}, \Omega, \phi, \mathbb{C}^H$) are computed separately and successively through an iterative approach.

Compared with the first algorithm proposed in Fig. 3 (blue box), one can observe that the microscale steps are replaced by making use of the database. Indeed, once the macroscale strain field $\bar{\boldsymbol{\varepsilon}}$ is computed, the value of the objective function defined in equation ((3)) is evaluated for each snapshot with given $\bar{\boldsymbol{\varepsilon}}$ from the macroscale. The snapshot leading to the best performance (that is the minimal value of the objective function (3)) is selected from the catalog database and its homogenized elasticity tensor \mathbb{C}^H is used to update the material properties at the macroscale. This approach involves to compute the objective function for each snapshot in the database without any FE computations. At each macro-iteration, the instantaneous selection of the best micro-architected material over the database is based on the compliance-weight minimization criterion with respect to the equation:

$$\int_{\Omega} \boldsymbol{\varepsilon}(\bar{\mathbf{u}}) : \mathbb{C}^H : \boldsymbol{\varepsilon}(\bar{\mathbf{u}}) d\Omega + \beta \phi \int_D d\Omega \quad (17)$$

This is done without any microscale FE computations. Indeed, each snapshot of the material catalog contains as stored information: the micro-structure topology (geometry), its homogenized stiffness

Algorithm 1. Alternate directions data assisted topology optimization algorithm

```

Input : macroscopic boundary conditions, mesh size and initial guesses for the
         topology, the catalog of microstructure  $\mathbb{C}_0$ , stopping criterion tolerance  $\bar{\epsilon}$ 
Output: macroscopic optimized topology with unique optimized
         micro-architected material

/* Initialization */
1 Set  $k = 0$ : initial micro-architected material assignment  $\mathbb{C}_k^H = \mathbb{C}_0^H, \Omega_0,$ 
2 while  $\epsilon > \bar{\epsilon}$  do
   /* Macroscale resolution */
3   Solve the macro-BVP for the current configuration design variables  $\Omega_k^H, \mathbb{C}_k^H$ 
4   Select the best microstructure in the database with respect to equation 17
5   Update material properties:  $\mathbb{C}_{k+1}^H$ 
6   Re-solve the macro-BVP for the new configuration  $\Omega_k, \mathbb{C}_{k+1}^H$ 
   /* Shape derivative */
7   Update the the level-set  $\psi_{k+1}$  and so  $\Omega_{k+1}$  with respect to equation (8) where
   the velocity function is evaluated with Appendix C (equation (51))
8   Compute the stopping criterion
9   Iterate  $k \leftarrow k + 1$ 
10 end

```

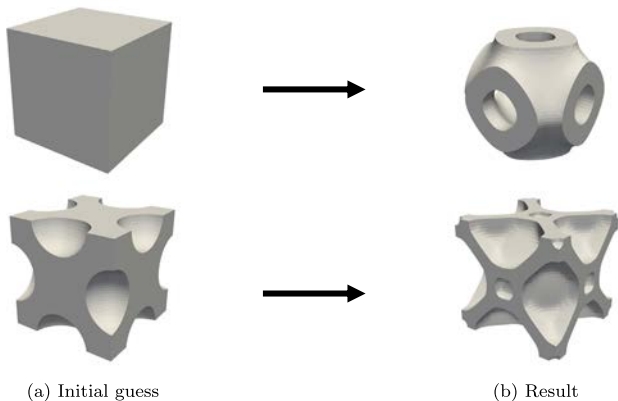


Fig. 7. Influence of the initial guess on the topology for the same prescribed elasticity tensor.

tensor \mathbb{C}^H and its volume fraction Φ . Since the trade-off parameter β is fixed by the user, and the macro-displacement $\bar{\mathbf{u}}$ as the structure volume $\int_D d\Omega$ are computed at the macroscale iteration, one has just to loop over the catalog snapshots (i.e. loop over the stored couples of (\mathbb{C}^H, Φ)) to obtain the best micro-structure that minimizes the compliance-weight functional (17). One can find in the literature some advanced methods to interpolate within the database to improve the numerical efficiency associated to this phase of the algorithm [61–63]. The next steps consist in recomputing the mechanical equilibrium with the updated microstructure and update the level-set. The stopping criterion is verified if the level-set does not evolve significantly in a few iteration:

$$\epsilon = \sum_{k=0}^m \frac{\max_{p \in 1..N} (\psi_{k+1}(p) - \psi_k(p))}{m}$$

where m is an arbitrary value that account for the stability of the level-set function ψ over the iterations and N is the number of point

of the level-set grid. The concurrent macro/micro optimization method using precomputed catalog is illustrated in the sequel for 3D cases.

Remark. The two-scales topology optimization driven by the Algorithm 1 leads *in fine* to the macroscopic topology Ω and the corresponding micro-architected topology selected from the catalog. The macroscopic mechanical fields, respecting the macroscopic BVP $G(\bar{\mathbf{u}}) = 0$, are also obtained. For mechanical post-processing purposes, one can thus use the macroscopic fields $(\bar{\mathbf{u}}, \bar{\boldsymbol{\varepsilon}}, \bar{\boldsymbol{\sigma}})$ to achieve a macroscopic analysis. An optional step can be added *a posteriori* to obtain the local mechanical fields $(\mathbf{u}, \boldsymbol{\varepsilon}, \boldsymbol{\sigma})$ and not only the macroscopic fields. This stage can be done using a localization operator \mathcal{A} (e.g. [64,48]) so that the down-scaling step is straightforward $\mathbf{u} = \mathcal{A}(\bar{\boldsymbol{\varepsilon}})$. Local mechanical analysis can be so achieved at fine scales.

4.3.1. Example 1

The admissible domain dimensions is $1\text{ m} \times 1\text{ m} \times 1\text{ m}$ discretized with $N^{\text{mac}} = 64000$ elements. The Dirichlet boundary conditions are homogeneous on the top surface and a pressure load of $P = 1\text{ Pa}$ is applied on the bottom (see Fig. 8). The β parameter is set to 0.1. The evolution of the objective function as well as the optimal micro-architected material is illustrated in Fig. 9.

It can be inferred from this figure that the concurrent macro/micro optimization follows a pattern that can be divided in three steps. During the first step (iteration < 50 in this example) the macroscale topology varies slowly and so does the macro-strain tensor that is used to select the best micro-architected material. Therefore, during this step, the micro structure does not change. In the second step ($50 < \text{iteration} < 300$) the macroscale topology has drastically evolved compared to the initial guess so that the optimal micro-architected material changes. However the variation of the homogenized mechanical properties of the micro-architected material also impacts the macroscale equilibrium and the macroscale strain tensor which leads to instability. This instability comes from the alternation of the micro-architected material between two candidates while the macroscale topology keeps evolving. The third step (iteration > 300) is reached when the macroscale topology has sufficiently evolved so the variation of the microscale material properties due to the alternation of the micro-architected material does not impact the macroscale strain tensor enough to change the micro-architected material.

The solid phase ratio obtained at the macroscale is 0.598 and the micro-architected material has a solid phase ratio of 0.4154. The global solid phase ratio is thus 0.248. The evolution

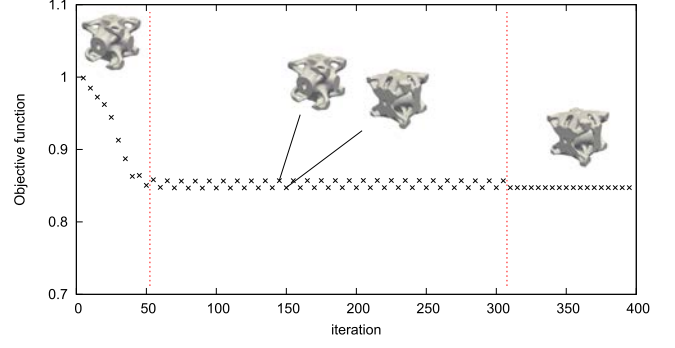


Fig. 9. Evolution of the objective function and the optimal micro architected material throughout the optimization process.

of the topology at the macroscale is illustrated for some iterations in Fig. 10.

The impact of the micro-architected database has been studied. A preliminary catalog containing only 200 snapshots has been firstly considered. For this configuration the algorithm fails to achieve the stop criterion. The catalog has been enriched afterwards with $N^{\text{snap}} = 1000$ snapshots which guarantees the two-scales convergence.

4.3.2. Example 2

The admissible domain dimensions is $1\text{ m} \times 1\text{ m} \times 2\text{ m}$ discretized with $N^{\text{mac}} = 16000$ elements. The Dirichlet boundary conditions are homogeneous on the left surface and pressure load of $P = 1\text{ Pa}$ is applied on the black highlighted part of the right surface (see Fig. 8). The β parameter that sets the compromise between the two criteria of the objective function (1) is set to 8. The evolution of the objective function as well as the optimal micro-architected material is illustrated in Fig. 12. Likewise Example 1, one can identify the different steps through the optimization. However for this example the convergence seems more complicated to reach since 4 different micro-architected materials are involved instead of 2 for Example 1. The non smoothness observed during the iterative process is partly due to the number of snapshots in the database. As mentioned in Section 4.3.1 the first multi-scale attempts were made with a database containing only $N^{\text{snap}} = 200$ snapshots. In this case, the algorithm failed to reach convergence because of the gap between the mechanical properties of the available materials. Even if the convergence of the proposed method is not guaranteed even for wider database, it is observed that increasing the

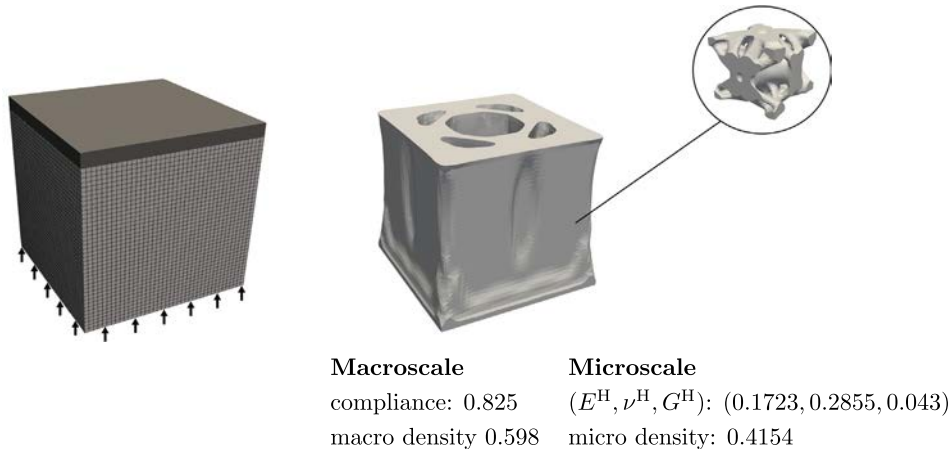


Fig. 8. Boundary conditions and macro optimal topology for Example 1. The corresponding optimal micro-topology is illustrated as the optimized design performances at the macro and micro scales (SI units).

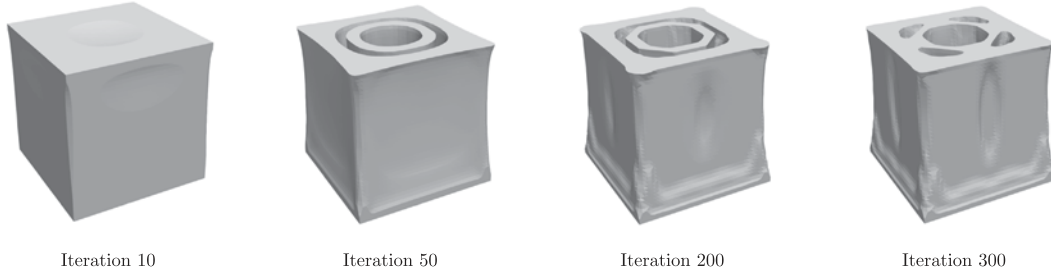


Fig. 10. Evolution of the macroscale topology for Example 2.

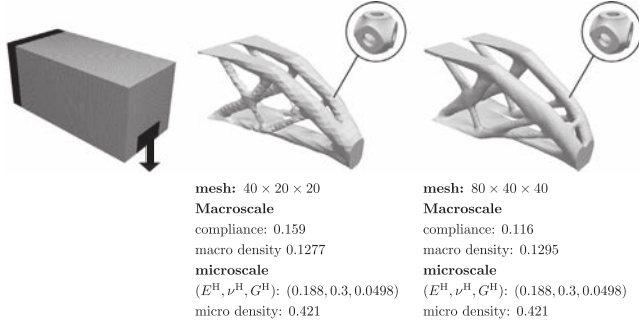


Fig. 11. Boundary conditions and macro optimal topology for Example 2. The corresponding optimal micro-topology is illustrated as the optimized design performances at the macro and micro scales (SI units).

number of snapshots improves the smoothness of the procedure. Nevertheless the material convergence is reached in 105 iterations. The discretization effect is studied with two mesh configurations ($40 \times 20 \times 20$ and $80 \times 40 \times 40$ elements). Fig. 11 illustrates the effect of the mesh refinement on the objective function. One can see that the selected micro-architected materials are the same independently of the mesh size. However, the corresponding compliance decreases with nearly 0.27% as the mesh size decreases. In order to study the convergence of the obtained result with respect to the mesh size, a more refined mesh case can be considered.

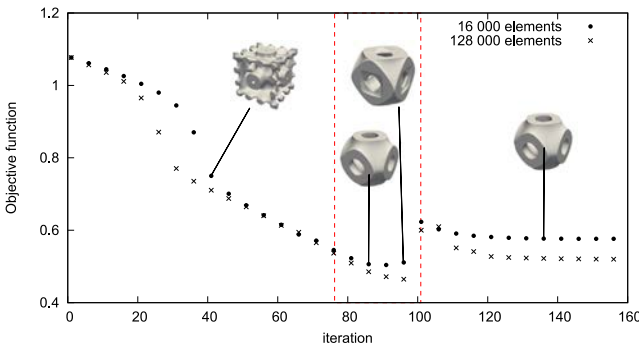


Fig. 12. Evolution of the objective function and the optimal micro architected material throughout the optimization process.

Table 2
Illustration of the topology optimization CPU for each scale.

Examples				
Mesh	160×80	80×80	$120 \times 60 \times 60$	$40 \times 40 \times 40$
Design variables	12800	6400	432000	64000
CPU	≈ 1.42 min	≈ 1 min	≈ 10 h	≈ 34 mn

Another feasible solution is to consider the topology obtained at the last iteration of the $80 \times 40 \times 40$ mesh case, then decrease the mesh size and re-start the optimization process. Such a solution allows to avoid expansive time computations. This solution has not been studied in the paper.

The solid phase ratio obtained at the macroscale is 0.1295 and the micro-architected material has a solid phase ratio of 0.421. Consequently the global solid phase ratio is 0.0545.

4.4. Algorithm complexity analysis

The number of operation to be performed for the studied multiscale problem is significantly reduced thanks to the data-assisted strategy. Indeed, the total CPU time needed for a standard multiscale topology optimization algorithm (blue box in Fig. 2) is the number of operation needed for $\mathcal{O}(N^{\text{mac}} \times N^{\text{mic}})$ design variables (for a structure sampled into N^{mac} elements containing each microstructures with N^{mic} elements). Table 2 illustrates the topology optimization CPU associated to each scale for some 2D and 3D cases. Hence, if one considers the 3D case example with a two-scale topology optimization, the total number of the two-scales design variables to be optimized is $\mathcal{O}(27648.10^6)$ with a CPU time reaching drastically a huge number of years. This is unaffordable and no practical even if using advanced computations techniques. In contrast, the proposed strategy has the advantage to run only FE computations for $\mathcal{O}(N^{\text{mac}} = 432.10^3)$ design variables since the design optimization of the microstructures is done offline and stored in the micro-architected catalog: at the offline step, one has to run $N^{\text{snap}} \ll N^{\text{mic}}$ computations for $\mathcal{O}(N^{\text{mic}} = 64.10^4)$ design variables. This is done once-for-all and stored in a material database which can be used after online for different macro-structure topology optimization problems. A high gain of CPU time is obtained as illustrated in Table 3.

Table 3
Example of CPU time for a 3D data-assisted multiscale topology optimization.

	off-line	on-line
data-assisted solver	$N^{\text{snap}} \times 34$ mn	10 h

5. Conclusion

In this paper, a two-scales optimization method is proposed for the design of 3D stiff and light structures incorporating porous micro-architected materials. This topology optimization is based on a level-set formulation using shape derivative for the shape optimization. To overcome the prohibitive computational costs of the coupled optimization of the two scales, a database assisted strategy is introduced. In a preliminary step, called ‘‘off line step’’, a catalog of optimal materials is built for a wide range of effective properties. Once a sufficient number of snapshots is computed, the database is consulted in the so called ‘‘on line step’’ to identify the best material from the catalog to minimize the multi-scale cost function.

The ability of this method to perform topology changes relaxes the impact of the choice of the initial guess for the topology. Nevertheless, for the same prescribed macroscopic elasticity tensor, using different initial topology could lead to different optimal topology and it is still an open question to link the efficiency of the optimal topology to the initial guess. The micro-architected material is considered to be ‘‘optimal’’ as long as the error between the prescribed constitutive tensor and the homogenized one is sufficiently small.

For the sake of simplicity, only cubic materials are considered in the catalog. A potential axis of improvement would be to extend the catalog to orthotropic materials and arguably fully anisotropic materials. Reduced order models (ROM) could be used too in order to increase the number of snapshots in the database with a reduced computational cost.

Declaration of Competing Interest

The authors declare that they have no known competing financial interests or personal relationships that could have appeared to influence the work reported in this paper.

Acknowledgement

The authors thank the financial support from the French Ministry of Higher Education, Research and Innovation.

Appendix A. Shape derivative of a functional

In Appendix A, the shape derivative method is applied to a generic functional $J(\Omega)$ that is expressed as the integral of a scalar function f over a domain Ω [35]. The aim is to define a velocity function $\mathbf{V}(\mathbf{x}(\mathbf{X}, t), t)$ that minimizes the cost function when a perturbation is applied to Ω .

Let the cost function J be defined as:

$$J(\Omega_t) = \int_{\Omega_t} f(\mathbf{x}(\mathbf{X}, t)) d\mathbf{x} \quad (18)$$

where $f(\mathbf{x}(\mathbf{X}), t)$ is a scalar function defined in Ω_t .

Differentiating J with respect to a variation of Ω reads:

$$DJ(\Omega) = \lim_{t \rightarrow 0} \frac{1}{t} \left(\int_{\Omega_t} f(\mathbf{x}(\mathbf{X}, t)) d\mathbf{x} - \int_{\Omega} f(\mathbf{X}) d\mathbf{X} \right) \quad (19)$$

A change of variable is then performed in Eq. (19) introducing $F(t)$:

$$F(t) = \frac{\partial \mathbf{x}}{\partial \mathbf{X}} = \nabla T_t(\mathbf{X}) \quad (20)$$

$$\begin{aligned} DJ(\Omega) &= \lim_{t \rightarrow 0} \frac{1}{t} \left(\int_{\Omega_t} f(\mathbf{x}(\mathbf{X}, t)) d\mathbf{x} - \int_{\Omega} f(\mathbf{X}) d\mathbf{X} \right) \\ &= \lim_{t \rightarrow 0} \frac{1}{t} \int_{\Omega} [(f \circ T_t)(\mathbf{X})F(t) - (f \circ T_0)(\mathbf{X})F(0)] d\mathbf{X} \\ &= \int_{\Omega} \lim_{t \rightarrow 0} \frac{1}{t} [(f \circ T_t)(\mathbf{X})F(t) - (f \circ T_0)(\mathbf{X})F(0)] d\mathbf{X} \\ &= \int_{\Omega} D[(f \circ T_t)(\mathbf{X})F(t)]_{t=0} d\mathbf{X} \end{aligned} \quad (21)$$

The term in the integral can be computed using classical continuum mechanical results:

$$\begin{aligned} D((f \circ T_t)(\mathbf{X})F(t)) &= D(f \circ T_t)(\mathbf{X})F(t) + (f \circ T_t)(\mathbf{X})DF(t) \\ &= \frac{\partial}{\partial \mathbf{x}} (f \circ T_t)(\mathbf{X})\mathbf{V}(\mathbf{x}(\mathbf{X}, t), t)F(t) \\ &\quad + (f \circ T_t)(\mathbf{X})F(t)\text{div}(\mathbf{V}(\mathbf{x}(\mathbf{X}, t), t)) \end{aligned} \quad (22)$$

At $t = 0$ since $F(0) = I$ where I is second order identity tensor, it comes:

$$\begin{aligned} DJ(\Omega) &= \int_{\Omega} \frac{\partial}{\partial \mathbf{x}} f(\mathbf{X}) \cdot \mathbf{V}(\mathbf{X}, 0) + f(\mathbf{X})\text{div}(\mathbf{V}(\mathbf{X}, 0)) d\mathbf{X} \\ &= \int_{\Omega} \text{div}(f(\mathbf{X})\mathbf{V}(\mathbf{X}, 0)) d\mathbf{X} \end{aligned} \quad (23)$$

Finally, the Green-Ostrogradski formula is applied:

$$DJ(\Omega) = \int_{\partial\Omega} f(\mathbf{X})\mathbf{V}(\mathbf{X}, 0)\mathbf{n} d\mathbf{X} \quad (24)$$

To decrease the cost function $J(\Omega)$ one can choose the velocity function of the perturbation T_t as $\mathbf{V}(\mathbf{X}, 0) = -f(\mathbf{X})\mathbf{n}$ which leads to:

$$DJ(\Omega) = \int_{\partial\Omega} -f(\mathbf{X})^2 d\mathbf{X} < 0 \quad (25)$$

Such a choice of \mathbf{V} ensures the decrease of the cost function.

Appendix B. Shape derivative of the microscale objective function

Details about the computation of the stationarity point for the augmented lagrangian function of the objective function at the microscale are given in this paragraph.

Eq. (5) illustrates that the cost function depends on several displacement fields solutions of the boundary value problems at the micro scale. Hence the augmented lagrangian function can be written as:

$$L(\Omega^m, \mathbf{v}, \mathbf{v}_1) = J^m(\Omega^m, \tilde{\mathbf{u}}) + G(\mathbf{v}, \mathbf{v}_1) \quad (26)$$

where $\mathbf{v} = \{\mathbf{v}^{(11)}, \mathbf{v}^{(12)}, \mathbf{v}^{(13)}, \mathbf{v}^{(22)}, \mathbf{v}^{(23)}, \mathbf{v}^{(33)}\}$, $\mathbf{v}_1 = \{\mathbf{v}_1^{(11)}, \mathbf{v}_1^{(12)}, \mathbf{v}_1^{(13)}, \mathbf{v}_1^{(22)}, \mathbf{v}_1^{(23)}, \mathbf{v}_1^{(33)}\}$ and $\tilde{\mathbf{u}} = \{\tilde{\mathbf{u}}^{(11)}, \tilde{\mathbf{u}}^{(12)}, \tilde{\mathbf{u}}^{(13)}, \tilde{\mathbf{u}}^{(22)}, \tilde{\mathbf{u}}^{(23)}, \tilde{\mathbf{u}}^{(33)}\}$ correspond to each imposed strain mode defined by Eq. (6) (3 modes for 2D cases and 6 modes for 3D cases) and $G(\mathbf{v}, \mathbf{v}_1)$ is a functional that enforces the micro scale equations corresponding to the variational principle for each deformation mode defined in (6):

$$G(\mathbf{v}, \mathbf{v}_1) = \sum_{ij} \int_{\Omega^m} \sigma(\mathbf{v}^{(ij)}) : \varepsilon(\mathbf{v}_1^{(ij)}) d\Omega^m \quad (27)$$

The Lagrangian functional defined in Eq. (26) can then be differentiated:

$$\begin{aligned} \delta L(\Omega^m, \mathbf{v}, \mathbf{v}_1) &= \frac{\partial L}{\partial \Omega^m} \delta \Omega^m + \sum_{ij} \frac{\partial L}{\partial \mathbf{v}^{(ij)}} \delta \mathbf{v}^{(ij)} + \sum_{ij} \frac{\partial L}{\partial \mathbf{v}_1^{(ij)}} \delta \mathbf{v}_1^{(ij)} = 0 \\ \forall (\delta \mathbf{v}^{(ij)}, \delta \mathbf{v}_1^{(ij)}, (i, j)) &\in \left(\mathcal{W}_{\mathbf{v}^{(ij)}}, \mathcal{W}_{\mathbf{v}_1^{(ij)}}, \{1, 2, 3\}^2 \right) \end{aligned} \quad (28)$$

where these functional spaces have good properties of regularity.

The terms of Eq. (28) are regrouped in three sets depending on $\delta \Omega^m$, each $\delta \mathbf{v}^{(ij)}$ and each $\delta \mathbf{v}_1^{(ij)}$ for all macro strain mode (ij) .

The terms depending on each $\delta \mathbf{v}_1^{(ij)}$ read:

$$\frac{\partial L}{\partial \mathbf{v}_1^{(ij)}} \delta \mathbf{v}_1^{(ij)} = \int_{\Omega^m} \sigma(\mathbf{v}^{(ij)}) : \frac{\partial \varepsilon(\mathbf{v}_1^{(ij)})}{\partial \mathbf{v}_1^{(ij)}} \delta \mathbf{v}_1^{(ij)} d\Omega^m = 0 \quad (29)$$

Eq. (29) can be rewritten using integration by parts and the constitutive law as:

$$-\int_{\Omega^m} \operatorname{div} \sigma(\mathbf{v}^{(ij)}) \delta \mathbf{v}_1^{(ij)} d\Omega^m + \int_{\partial\Omega^m} \sigma(\mathbf{v}^{(ij)}) \mathbf{n} \delta \mathbf{v}_1^{(ij)} dS = 0 \quad (30)$$

Eq. (30) implies that each virtual displacement field $\mathbf{v}^{(ij)}$ is the solution of the boundary value problem at the microscale associated to a macro strain mode (ij) .

The terms of Eq. (28) depending on $\delta \mathbf{v}^{(pq)}$ read:

$$\begin{aligned} \frac{\partial L}{\partial \mathbf{v}^{(ij)}} \delta \mathbf{v}^{(ij)} &= \frac{2}{|\Omega^m|} \times \sum_{kl} \eta_{ijkl} \left(C_{ijkl}^H - C_{ijkl}^T \right) \int_{\Omega^m} \frac{\sigma(\mathbf{v}^{(ij)})}{\partial \mathbf{v}^{(ij)}} \delta \mathbf{v}^{(ij)} : \varepsilon(\mathbf{v}^{(kl)}) d\Omega^m \\ &+ \int_{\Omega^m} \frac{\partial \sigma(\mathbf{v}^{(ij)})}{\partial \mathbf{v}^{(ij)}} \delta \mathbf{v}^{(ij)} : \varepsilon(\mathbf{v}_1^{(ij)}) d\Omega^m = 0 \end{aligned} \quad (31)$$

Eq. (31) can be rewritten using the constitutive law:

$$\begin{aligned} \frac{\partial L}{\partial \mathbf{v}^{(ij)}} \delta \mathbf{v}^{(ij)} &= \sum_{kl} Q_{ijkl} \int_{\Omega^m} \sigma(\mathbf{v}^{(kl)}) : \varepsilon(\delta \mathbf{v}^{(ij)}) d\Omega^m \\ &+ \int_{\Omega^m} \sigma(\mathbf{v}_1^{(ij)}) : \varepsilon(\delta \mathbf{v}^{(ij)}) d\Omega^m = 0 \end{aligned} \quad (32)$$

where:

$$Q_{ijkl} = \frac{2}{|\Omega^m|} \times \eta_{ijkl} \left(C_{ijkl}^H - C_{ijkl}^T \right) \quad (33)$$

Eq. (32) can be rewritten using integration by parts:

$$\begin{aligned} \frac{\partial L}{\partial \mathbf{v}^{(ij)}} \delta \mathbf{v}^{(ij)} &= \sum_{kl} Q_{ijkl} \left[- \int_{\Omega^m} \operatorname{div} \sigma(\mathbf{v}^{(kl)}) \delta \mathbf{v}^{(ij)} d\Omega^m + \int_{\partial\Omega^m} \sigma(\mathbf{v}^{(kl)}) \mathbf{n} dS \right] \\ &- \int_{\Omega^m} \operatorname{div} \sigma(\mathbf{v}_1^{(ij)}) \delta \mathbf{v}^{(ij)} d\Omega^m + \int_{\partial\Omega^m} \sigma(\mathbf{v}_1^{(ij)}) \mathbf{n} dS = 0 \end{aligned} \quad (34)$$

Finally, Eq. (34) leads to the determination of the Lagrange multipliers $\mathbf{v}_1^{(ij)}$:

$$\varepsilon(\mathbf{v}_1^{(ij)}) = - \sum_{kl} Q_{ijkl} \varepsilon(\mathbf{v}^{(ij)}) \quad (35)$$

Using Eqs. (30) and (35), one can compute the stationarity point of the Lagrangian function. The method presented in Appendix A can then be applied to the Lagrangian function with respect to the stationarity point. Using a conventional result of shape derivative [35]:

$$D(A(\Omega) \times B(\Omega)) = B(\Omega) \times DA(\Omega) + A(\Omega) \times DB(\Omega) = 0 \quad (36)$$

Finally, the shape derivative of L reads:

$$DL(\Omega^m) = \int_{\partial\Omega^m} \sum_{ijkl} Q_{ijkl} \sigma(\mathbf{v}^{(ij)}) : \varepsilon(\mathbf{v}^{(kl)}) \mathbf{V} \cdot \mathbf{n} dS \quad (37)$$

Appendix C. Shape derivative of the macroscale objective function

The augmented Lagrangian functional for the macro scale problem is stated as:

$$L(\Omega^M, \mathbf{v}, \mathbf{v}_1, \mathbf{r}) = J^M(\Omega^M, \mathbf{v}) + G(\mathbf{v}, \mathbf{v}_1, \mathbf{r}) \quad (38)$$

where $G(\mathbf{v}, \mathbf{v}_1, \mathbf{r})$ is a functional that enforces the macro scale Eqs. (39) corresponding to the variational principle:

$$\left\{ \begin{array}{l} \operatorname{div} \sigma = 0 \quad \text{on } \Omega^M \\ \sigma \cdot \mathbf{n} = \bar{\mathbf{t}}_N \quad \text{on } \Gamma_N \\ \mathbf{u} = \mathbf{0} \quad \text{on } \Gamma_D \\ \sigma \cdot \mathbf{n} = \mathbf{0} \quad \text{on } \Gamma \cap \{\Gamma_N \cup \Gamma_D\} \\ \sigma = \mathbb{C} : \varepsilon \end{array} \right. \quad (39)$$

where Γ_N is the Neumann boundary where the external forces are applied, Γ_D is the Dirichlet boundary where the displacement are

prescribed. For the sake of simplicity, the prescribed displacement are of nil value.

$$G(\mathbf{v}, \mathbf{v}_1, \mathbf{r}) = \int_{\Omega^M} \sigma : \varepsilon(\mathbf{v}_1) d\Omega^M - \int_{\Gamma_N} \bar{\mathbf{t}}_N \cdot \mathbf{v}_1 dS - \int_{\Gamma_D} \mathbf{v}_1 \cdot \mathbf{r} dS \quad (40)$$

To compute the shape derivative of the Lagrangian function L defined in Eq. (38) the method presented in Appendix A can be directly applied since the displacement field $\bar{\mathbf{u}}$ subject to the macro scale equations has been replaced by a virtual displacement \mathbf{v} . Nevertheless it is necessary to compute the virtual displacement \mathbf{v} and the Lagrange multipliers \mathbf{v}_1 and \mathbf{r} by differentiating L :

$$\delta L(\Omega^M, \mathbf{v}, \mathbf{v}_1, \mathbf{r}) = \frac{\partial L}{\partial \mathbf{v}} \delta \mathbf{v} + \frac{\partial L}{\partial \mathbf{v}_1} \delta \mathbf{v}_1 + \frac{\partial L}{\partial \mathbf{r}} \delta \mathbf{r} = 0 \quad (41)$$

$$\forall (\delta \mathbf{v}, \delta \mathbf{v}_1, \delta \mathbf{r}) \in (\mathcal{U}_{\mathbf{v}}, \mathcal{U}_{\mathbf{v}_1}, \mathcal{U}_{\mathbf{r}})$$

where these functional spaces have good properties of regularity.

Developing Eq. (41) reads:

$$\begin{aligned} \delta L(\Omega^M, \mathbf{v}, \mathbf{v}_1, \mathbf{r}) &= \int_{\Gamma_N} \bar{\mathbf{t}}_N \cdot \delta \mathbf{v} dS + \int_{\Omega^M} \frac{\partial \sigma}{\partial \mathbf{v}} \delta \mathbf{v} : \varepsilon(\mathbf{v}_1) d\Omega^M \\ &+ \int_{\Omega^M} \sigma : \varepsilon(\delta \mathbf{v}_1) d\Omega^M - \int_{\Gamma_N} \bar{\mathbf{t}}_N \cdot \delta \mathbf{v}_1 dS - \int_{\Gamma_D} \delta \mathbf{v}_1 \cdot \mathbf{r} dS \\ &- \int_{\Gamma_D} \mathbf{v}_1 \cdot \delta \mathbf{r} dS \end{aligned} \quad (42)$$

The terms of Eq. (42) are regrouped in three sets depending on $\delta \mathbf{v}$, $\delta \mathbf{v}_1$ and $\delta \mathbf{r}$.

The first set depending on $\delta \mathbf{v}$ introducing the constitutive law reads:

$$\int_{\Gamma_N} \bar{\mathbf{t}}_N \cdot \delta \mathbf{v} dS + \int_{\Omega^M} \mathbb{C}^M \frac{\partial \varepsilon}{\partial \mathbf{v}} \delta \mathbf{v} : \varepsilon(\mathbf{v}_1) d\Omega^M = 0 \quad (43)$$

Considering that:

$$\delta \varepsilon = \varepsilon(\delta \mathbf{v}) \quad (44)$$

and using integration by parts, Eq. (43) can be rewritten as:

$$\int_{\Gamma_N} \bar{\mathbf{t}}_N \cdot \delta \mathbf{v} dS - \int_{\Omega^M} \operatorname{div}(\sigma(\mathbf{v}_1)) \cdot \delta \mathbf{v} d\Omega^M + \int_{\partial\Omega^M} \sigma(\mathbf{v}_1) \mathbf{n} \cdot \delta \mathbf{v} dS = 0 \quad (45)$$

Regrouping the terms on the bounds $\partial\Omega^M$ reads:

$$\int_{\Gamma_N} (\bar{\mathbf{t}}_N + \sigma(\mathbf{v}_1) \mathbf{n}) \cdot \delta \mathbf{v} dS - \int_{\Omega^M} \operatorname{div}(\sigma(\mathbf{v}_1)) \cdot \delta \mathbf{v} d\Omega^M + \int_{\Gamma_D} \sigma(\mathbf{v}_1) \mathbf{n} \cdot \delta \mathbf{v} dS = 0 \quad (46)$$

Eq. (46) implies that $\mathbf{v}_1 = -\mathbf{v}$ in the domain Ω^M and on the Neumann bound Γ_N . The problem is self-adjoint.

The second set of Eq. (42) depending on $\delta \mathbf{v}_1$ using integration by parts reads:

$$-\int_{\Omega^M} \operatorname{div}(\sigma) \cdot \delta \mathbf{v}_1 d\Omega^M + \int_{\partial\Omega^M} \sigma \mathbf{n} \cdot \delta \mathbf{v}_1 dS - \int_{\Gamma_N} \bar{\mathbf{t}}_N \cdot \delta \mathbf{v}_1 dS - \int_{\Gamma_D} \mathbf{r} \cdot \delta \mathbf{v}_1 dS = 0 \quad (47)$$

Regrouping the terms on the bounds $\partial\Omega^M$ reads:

$$\begin{aligned} &-\int_{\Omega^M} \operatorname{div}(\sigma) \cdot \delta \mathbf{v}_1 d\Omega^M + \int_{\Gamma_N} (\sigma \mathbf{n} - \bar{\mathbf{t}}_N) \cdot \delta \mathbf{v}_1 dS \\ &+ \int_{\Gamma_D} (\sigma \mathbf{n} - \mathbf{r}) \cdot \delta \mathbf{v}_1 dS + \int_{\partial\Omega^M \setminus \Gamma_N \setminus \Gamma_D} \sigma \mathbf{n} \cdot \delta \mathbf{v}_1 dS = 0 \end{aligned} \quad (48)$$

Eq. (48) implies that the virtual displacement field \mathbf{v} is the solution of the macro boundary value problem. The third set of Eq. (42) depending on $\delta \mathbf{r}$ reads:

$$\int_{\Gamma_D} \mathbf{v}_1 \cdot \delta \mathbf{r} dS = 0 \quad (49)$$

Eq. (49) implies that $\mathbf{v}_1 = \mathbf{0}$ on the Dirichlet boundary Γ_D . Combining Eqs. (46, 48,49), the Lagrangian functional defined in Eq. (38) can be rewritten as:

$$L(\Omega^M, \mathbf{v}, \mathbf{r}) = \int_{\Omega^M} (\beta - \sigma : \bar{\varepsilon}) d\Omega^M + 2 \int_{\Gamma_N} \bar{\mathbf{t}}_N \cdot \mathbf{v} + \int_{\Gamma_D} \mathbf{r} \cdot \mathbf{v} dS \quad (50)$$

At this point, the stationarity point of the lagrangian functional (38) can be computed and the method presented in Appendix A can directly be applied to the Lagrangian functional L . Considering that boundaries with prescribed displacement or traction forces have zero velocity, the velocity function can be computed using the shape derivative of L :

$$DL(\Omega^M) = \int_{\partial\Omega^M} (\beta - \sigma : \bar{\varepsilon}) \mathbf{V} \cdot \mathbf{n} dS \quad (51)$$

References

- [1] Zhou M, Alexandersen J, Sigmund O, Pedersen CB. Industrial application of topology optimization for combined conductive and convective heat transfer problems. *Struct Multidiscipl Optimiz* 2016;54(4):1045–60.
- [2] Andreassen E, Lazarov BS, Sigmund O. Design of manufacturable 3d extremal elastic microstructure. *Mech Mater* 2014;69(1):1–10.
- [3] Deng X, Wang Y, Yan J, Liu T, Wang S. Topology optimization of total femur structure: application of parameterized level set method under geometric constraints. *J Mech Des* 2016;138(1):011402.
- [4] Favre J, Lohmuller P, Piotrowski B, Kenzari S, Laheurte P, Meraghni F. A continuous crystallographic approach to generate cubic lattices and its effect on relative stiffness of architected materials. *Addit Manuf* 2018;21:359–68.
- [5] Bendsoe MP, Kikuchi N. Generating optimal topologies in structural design using a homogenization method. *Comput Methods Appl Mech Eng* 1988;71(2):197–224.
- [6] Wang X, Mei Y, Wang MY. Level-set method for design of multi-phase elastic and thermoelastic materials. *Int J Mech Mater Des* 2004;1(3):213–39.
- [7] Gao T, Zhang W. Topology optimization involving thermo-elastic stress loads. *Struct Multidiscipl Optimiz* 2010;42(5):725–38.
- [8] Yoon GH, Jensen JS, Sigmund O. Topology optimization of acoustic-structure interaction problems using a mixed finite element formulation. *Int J Numer Methods Eng* 2007;70(9):1049–75.
- [9] Yoon GH. Acoustic topology optimization of fibrous material with delany-bazley empirical material formulation. *J Sound Vib* 2013;332(5):1172–87.
- [10] Xia L, Breitkopf P. Multiscale structural topology optimization with an approximate constitutive model for local material microstructure. *Comput Methods Appl Mech Eng* 2015;286:147–67.
- [11] Allaire G, Jouve F, Toader A-M. Structural optimization using sensitivity analysis and a level-set method. *J Comput Phys* 2004;194(1):363–93.
- [12] Allaire G, De Gournay F, Jouve F, Toader A-M. Structural optimization using topological and shape sensitivity via a level set method. *Control Cybernet* 2005;34(1):59.
- [13] Sigmund O. On the design of compliant mechanisms using topology optimization. *J Struct Mech* 1997;25(4):493–524.
- [14] Yamada T, Izui K, Nishiwaki S, Takezawa A. A topology optimization method based on the level set method incorporating a fictitious interface energy. *Comput Methods Appl Mech Eng* 2010;199(45–48):2876–91.
- [15] Wang S, Lim KM, Khoo BC, Wang MY. An extended level set method for shape and topology optimization. *J. Comput. Phys.* 2007;221(1):395–421.
- [16] Aage N, Lazarov BS. Parallel framework for topology optimization using the method of moving asymptotes. *Struct Multidiscipl Optimiz* 2013;47(4):493–505.
- [17] Sigmund O. Materials with prescribed constitutive parameters: an inverse homogenization problem. *Int J Solids Struct* 1994;31(17):2313–29.
- [18] Amstutz S, Giusti S, Novotny A, de Souza Neto E. Topological derivative for multi-scale linear elasticity models applied to the synthesis of microstructures. *Int J Numer Meth Eng* 2010;84(6):733–56.
- [19] Gao J, Li H, Gao L, Xiao M. Topological shape optimization of 3d micro-structured materials using energy-based homogenization method. *Adv Eng Softw* 2018;116:89–102.
- [20] Vogiatzis P, Chen S, Wang X, Li T, Wang L. Topology optimization of multi-material negative poisson ratio metamaterials using a reconciled level set method. *Comput Aided Des* 2017;83:15–32.
- [21] Kato J, Yachi D, Kyoya T, Terada K. Micro-macro concurrent topology optimization for nonlinear solids with a decoupling multiscale analysis. *Int J Numer Meth Eng* 2018;113(8):1189–213.
- [22] Groen JP, Sigmund O. Homogenization-based topology optimization for high-resolution manufacturable microstructures. *Int J Numer Meth Eng* 2018;113(8):1148–63.
- [23] Zheng J, Luo Z, Li H, Jiang C. Robust topology optimization for cellular composites with hybrid uncertainties. *Int J Numer Meth Eng* 2018;115(6):695–713.
- [24] Li H, Luo Z, Gao L, Qin Q. Topology optimization for concurrent design of structures with multi-patch microstructures by level sets. *Comput Methods Appl Mech Eng* 2018;331:536–61.
- [25] Wang L, Cai Y, Liu D. Multiscale reliability-based topology optimization methodology for truss-like microstructures with unknown-but-bounded uncertainties. *Comput Methods Appl Mech Eng* 2018;339:358–88.
- [26] Gaynor AT, Meisel NA, Williams CB, Guest JK. Multiple-material topology optimization of compliant mechanisms created via polyjet three-dimensional printing. *J Manuf Sci Eng* 2014;136(6).
- [27] Sanders ED, Aguiló MA, Paulino GH. Multi-material continuum topology optimization with arbitrary volume and mass constraints. *Comput Methods Appl Mech Eng* 2018;340:798–823.
- [28] Zhang XS, Paulino GH, Ramos Jr AS. Multimaterial topology optimization with multiple volume constraints: Combining the zpr update with a ground-structure algorithm to select a single material per overlapping set. *Int J Numer Meth Eng* 2018;114(10):1053–73.
- [29] Rozvany GI. A critical review of established methods of structural topology optimization. *Struct Multidiscipl Optimiz* 2009;37(3):217–37.
- [30] Bendsoe M, Sigmund O. *Topology optimization: Theory, methods and applications*; 2003. ISBN: 3-540-42992-1.
- [31] Sigmund O. A 99 line topology optimization code written in matlab. *Struct Multidiscipl Optimiz* 2001;21(2):120–7.
- [32] Zhang W, Yuan J, Zhang J, Guo X. A new topology optimization approach based on moving morphable components (mmc) and the ersatz material model. *Struct Multidiscipl Optimiz* 2016;53(6):1243–60.
- [33] Sethian JA. *Level set methods, evolving interfaces in geometry, fluid mechanics computer vision, and materials sciences*. Cambridge Monographs on Applied and Computational Mathematics 1996;3.
- [34] Peng D, Merriman B, Osher S, Zhao H, Kang M. A pde-based fast local level set method. *J Comput Phys* 1999;155(2):410–38.
- [35] Sokolowski J, Zolesio J-P. *Introduction to shape optimization. In: Introduction to Shape Optimization*. Springer; 1992. p. 5–12.
- [36] Otomori M, Yamada T, Izui K, Nishiwaki S. Matlab code for a level set-based topology optimization method using a reaction diffusion equation. *Struct Multidiscipl Optimiz* 2015;51(5):1159–72.
- [37] Milton G, Cherkaev A. Which elasticity tensors are realizable? *J Eng Mater Technol* 1995;117:483–93.
- [38] Czarnecki S, Lukasiak TL. The isotropic and cubic material designs. recovery of the underlying microstructures appearing in the least compliant continuum bodies. *Materials (Basel)* 2017;10(10):1137.
- [39] Ferrer A, Oliver J, Cante JC, Lloberas-Valls O. Vademecum-based approach to multi-scale topological material design. *Adv Model Simul Eng Sci* 2016;3(1):23.
- [40] Christian S, Bernd B, Jan R, Steve M, Chiara D, Markus G. Microstructures to control elasticity in 3d printing. *ACM Trans Graph (TOG)* 2015;34.
- [41] Long K, Wang X, Gu X. Concurrent topology optimization for minimization of total mass considering load-carrying capabilities and thermal insulation simultaneously. *Acta Mech Sin* 2018;34(2):315–26.
- [42] Panetta J, Rahimian A, Zorin D. Worst-case stress relief for microstructures. *ACM Trans Graph* 2017;36(4):1–16.
- [43] Tozoni D, Dumas J, Jlanh Z, Panetta J, Panozzo D, Zorin D. A low-parametric rhombic microstructure family for irregular lattices. *ACM Trans Graph (TOG)* 2020;39(4):101.
- [44] Tromme E, Kawamoto A, Guest JK. Topology optimization based on reduction methods with applications to multiscale design and additive manufacturing. *Front Mech Eng* 2020;15(1):151–65.
- [45] Geers M, Kouznetsova V, Brekelmans W. *Multi-scale modelling: Computational homogenization in solid mechanics*. Eindhoven University of Technology; 2003.
- [46] de Souza Neto EA, Feijóo RA, Novotny A. *Variational foundations of large strain multiscale solid constitutive models: kinematical formulation*. Advanced computational materials modeling: from classical to multi-scale techniques-scale techniques; 2011.
- [47] Michailidis G. *Manufacturing constraints and multi-phase shape and topology optimization via a level-set method*. Ph.D. thesis; 2014.
- [48] Michel J-C, Moulinec H, Suquet P. Effective properties of composite materials with periodic microstructure: a computational approach. *Comput Methods Appl Mech Eng* 1999;172(1–4):109–43.
- [49] Cea J, Garreau S, Guillaume P, Masmoudi M. The shape and topological optimizations connection. *Comput Methods Appl Mech Eng* 2000;188(4):713–26.
- [50] Zhu B, Skouras M, Chen D, Matusik W. Two-scale topology optimization with microstructures. *ACM Trans Graph (TOG)* 2017;36(4):1.
- [51] Auffray N, Le Quang H, He Q-C. Matrix representations for 3d strain-gradient elasticity. *J Mech Phys Solids* 2013;61(5):1202–23.
- [52] Walpole L. *Fourth-rank tensors of the thirty-two crystal classes: multiplication tables*. *Proc R Soc Lond Math Phys Sci* 1984;391(1800):149–79.
- [53] Zhu W, Blal N, Cunsolo S, Baillis D. Micromechanical modeling of effective elastic properties of open-cell foam. *Int J Solids Struct* 2017;115:61–72.
- [54] Hashin Z, Shtrikman S. A variational approach to the theory of the effective magnetic permeability of multiphase materials. *J Appl Phys* 1962;33(10):3125–31.
- [55] Kantor Y, Bergman D. Improved rigorous bounds on the effective elastic moduli of a composite material. *J Mech Phys Solids* 1984;32(1):41–62.
- [56] Cohen I. Simple algebraic approximations for the effective elastic moduli of cubic arrays of spheres. *J Mecap Phys Solids* 2004;52(9):2167–83.

- [57] Milton G, Briane M, Harutyunyan D. On the possible effective elasticity tensors of 2-dimensional and 3-dimensional printed materials. *Math Mech Complex Syst* 2017;5(1):41–94.
- [58] Sigmund O, Petersson J. Numerical instabilities in topology optimization: a survey on procedures dealing with checkerboards, mesh-dependencies and local minima. *Struct Optimiz* 1998;16(1):68–75.
- [59] Bertsch C, Csilino AP, Calvo N. Topology optimization of three-dimensional load-bearing structures using boundary elements. *Adv Eng Softw* 2010;41(5):694–704.
- [60] Jeong S, Lim S, Min S. Level-set-based topology optimization using remeshing techniques for magnetic actuator design. *IEEE Trans Magn* 2015;52(3):1–4.
- [61] Canales D, Leygue A, Chinesta F, González D, Cueto E, Feulvarch E, Bergheau J-M, Huerta A. Vademecum-based gfem (v-gfem): optimal enrichment for transient problems. *Int J Numer Meth Eng* 2016;108(9):971–89.
- [62] Amsallem D, Farhat C. Interpolation method for adapting reduced-order models and application to aeroelasticity. *AIAA J* 2008;46(7):1803–13.
- [63] Lu Y, Blal N, Gravouil A. Multi-parametric space-time computational vademecum for parametric studies: Application to real time welding simulations. *Finite Elem Anal Des* 2018;139:62–72.
- [64] Blal N, Gravouil A. Non-intrusive data learning based computational homogenization of materials with uncertainties. *Comput Mech* 2019:1–22.